PUBLICATIONS OF THE ASTRONOMICAL SOCIETY OF THE PACIFIC, **126**:380–385, 2014 April

A Sideband-separating Receiver with a Calibrated Digital If-Hybrid Spectrometer for the Millimeter Band

R. RODRÍGUEZ,[1] R. FINGER,[2] F. P. MENA,[1] NICOLÁS REYES,[1] ERNEST MICHAEL,[1] AND LEONARDO BRONFMAN[2]

Received 2014 January 03; accepted 2014 March 04; published 2014 March 28

ABSTRACT. Due to its advantages over other configurations, sideband-separating receivers are usually preferred for radio astronomy, particularly in the presence of high atmospheric noise. However, even with all the advances that have been made in recent years in the field of receiver technology, one of the most important figures of merit for this kind of receiver, the sideband rejection ratio, is still relatively low and typically around 10 to 20 dB. This is because keeping low amplitude and phase imbalances over large RF and IF bands is extremely difficult. In order to overcome this problem, it has been suggested that by introducing a digital back-end that mimics the performance of an IF-hybrid, such imbalances can be calibrated out. Until now, this has been demonstrated only at very low RF frequencies (below 4 GHz). Here, for the first time, we demonstrate that this technique can be applied at higher frequencies. We have implemented a sideband-separating receiver with a calibrated digital IF-hybrid spectrometer for the 3 mm band, and have demonstrated that, even in the presence of large imbalances of individual components, sideband ratios above 35 dB can be obtained in the entire RF band.

Online material: color figures.

1. INTRODUCTION

A coherent radio astronomical receiver can be implemented using different configurations—double sideband (DSB), sideband separating (2SB), or single sideband (SSB)—each having its advantages and disadvantages. The DSB configuration is the simplest but has the problem of superposition of the lower (LSB) and the upper sidebands (USB) in the intermediate frequency (IF). The SSB configuration avoids the problem of spectrum overlap in the IF by adding a filter before the mixing process. However, half of the radio frequency (RF) spectrum is lost, and making tunable filters at millimeter wavelengths is still very difficult. The use of the 2SB configuration implies an increase in the number of components and complexity, but makes it possible to observe the two sidebands simultaneously, reducing the noise and increasing the bandwidth of the observations. The 2SB configuration, presented in Figure 1*a*, has the inconvenience that the sideband rejection depends highly on the amplitude and phase imbalance of the entire system. In order to minimize the imbalance, the total electrical length must be the same in the two branches of the system. Mixers must have similar behavior, and hybrids and power splitters must perform very close to their nominal design. Achieving all of this over wide RF and IF ranges is in practice very difficult.

There are two ways of defining the sideband rejection ratio in a receiver. To understand this, let us consider Figure 1*b*, where we show schematically the signal flow from the RF input to the IF outputs (Kerr et al. 2001). Although in a real receiver there is only one RF input, for the sake of clarity Figure 1*b* represents the two sidebands as two different RF inputs, U and L. The downconverted signals, on the other hand, are obtained at outputs u and l. In a perfect receiver, these outputs would correspond only to USB and LSB, respectively. In the presence of imbalances we can, therefore, define two different sideband rejection ratios. One (r_U, r_L) measures the ammount of power from a signal in a given RF sideband delivered to the incorrect IF output, i.e.,

$$r_U = \frac{G_{uU}}{G_{lU}}; \qquad r_L = \frac{G_{lL}}{G_{uL}}. \tag{1}$$

The other definition (R_u, R_l) measures the ammount of power at a given IF output coming from a signal of equal power in the incorrect sideband, i.e.,

$$R_u = \frac{G_{uU}}{G_{uL}}; \qquad R_l = \frac{G_{lL}}{G_{lU}}. \tag{2}$$

In the case of a high IF, these definitions can give different results. In fact, the latter, is the relevant figure of merit in astronomical receivers.

In a simple model, where both definitions are identical, the sideband rejection ratio is given by (Kooi 2008)

[1] Electrical Engineering Department, University of Chile, Avenida Tupper 2007, Santiago 8370451, Chile; rrodrigu@ing.uchile.cl.

[2] Astronomy Department, University of Chile, Camino el Observatorio 1515, Las Condes, Santiago 7591245, Chile.

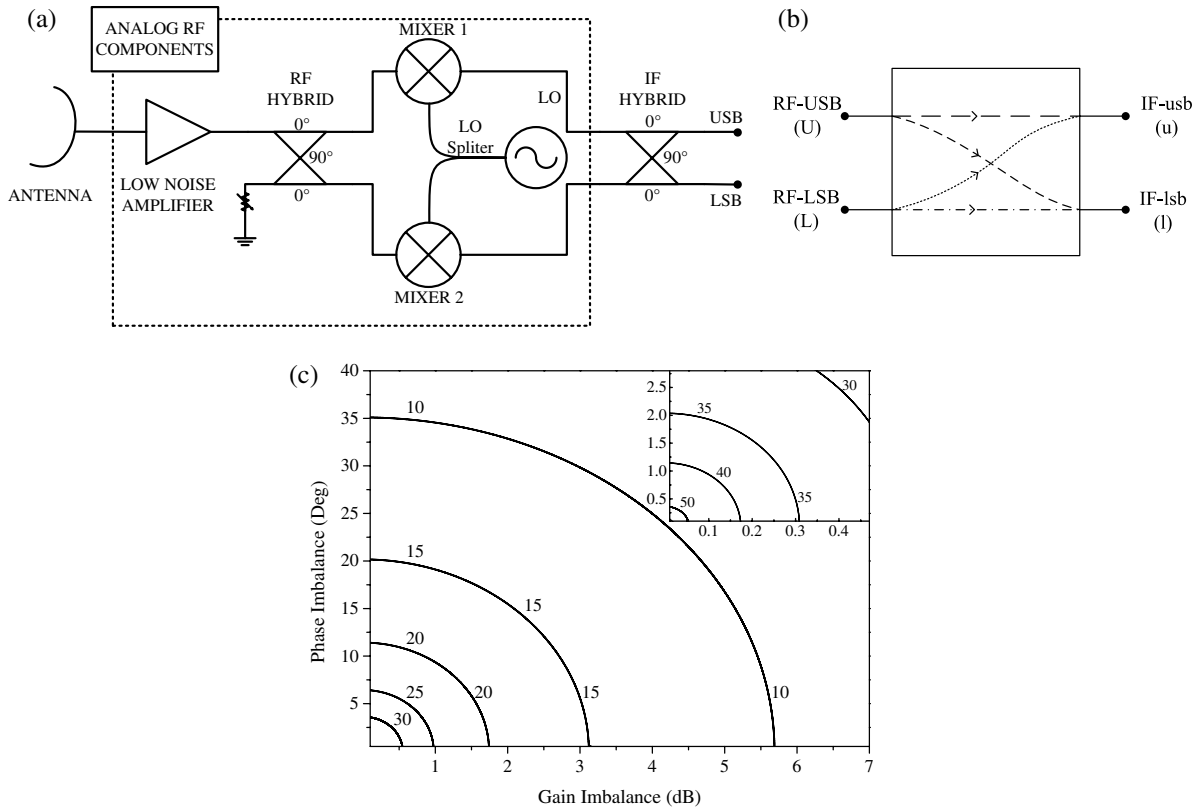

FIG. 1.—(*a*) Layout of the 2SB configuration. The amplified RF signal is divided in the RF hybrid into two signals of equal amplitude but with 90° phase difference. Then, both signals are down-converted in mixers in phase by the same LO. Finally, the down-converted signals are fed into an IF hybrid whose outputs give the desired LSB and USB IF signals. When the digital backend is used, the IF hybrid is replaced by an amplification stage and a digital board (in this case, a FPGA-based platform). (*b*) Schematic of the flow of the RF sidebands into the IF outputs used to define the sideband ratios R and r. (*c*) Sideband rejection ratio (in dB) for different phase and gain imbalances as calculated from eq. (3). The inset shows the rejection ratio for imbalances below 0.5 dB and 3°.

$$RR = -10 \times \log\left(\frac{1 - 2\sqrt{G}\cos\phi + G}{1 + 2\sqrt{G}\cos\phi + G}\right) \qquad (3)$$

where G and ϕ are the total amplitude and phase imbalances, respectively. Figure 1*c* illustrates how the rejection ratio is affected by the imbalances. Evidently, for low values of G and ϕ it is possible to obtain high sideband rejection. Modern all-analog receivers (Vassilev et al. 2004; Dindo et al. 2005; Sobis 2011; Mena et al. 2011; Mahieu et al. 2012; Maier et al. 2012) achieve rejections between 10 to 20 dB, demonstrating that achieving imbalances better than 20° and 3 dB is difficult over wide frequency ranges. A modern way to overcome this problem is to implement the IF hybrid digitally. In this way, the imbalances can be, to a large extent, calibrated out. Offline (Morgan and Fisher 2010) and real-time (Finger et al. 2013) implementations of this concept have been demonstrated, but only applied to low-frequency RF bands (below 4 GHz). In this article, we demonstrate that this concept can be applied at millimeter wavelengths (80–100 GHz) and demonstrate that sideband-rejection ratios greater than 35 dB can be achieved even in the presence of large imbalances. The rest of the article is structured as follows. Section 2 describes briefly the analog front end and the digital back end of the receiver. In § 3, we present the experiment and the methodology in the measurements. Then, in §§ 4 and 5, we present the results and conclusions, respectively.

2. RECEIVER DESCRIPTION

The receiver used in this work is a prototype for the 1.2 m Southern Millimeter Wave Telescope located at Cerro Calán, Chile (Rodrguez et al. 2012). This prototype follows the layout of Figure 1 which is similar to most modern sideband-separating receivers (Claude et al. 2000). It has a Hot Electron Mobility Transistor (HEMT) amplifier, an isolator, a RF hybrid, two W-band mixers and an IF hybrid. Note that the mixers and the IF hybrid are commercial components, while the RF hybrid and Local Oscillator (LO) splitter were designed and constructed at our facilities. This receiver was designed to work in the RF range from 84 to 116 GHz, with an IF between 0.1 and 3 GHz, although the final range achieved was 80 to 100 GHz at room temperature, limited only by the commercial mixers. A full characterization of an improved version of the front end at cryogenic temperatures will be presented elsewhere.

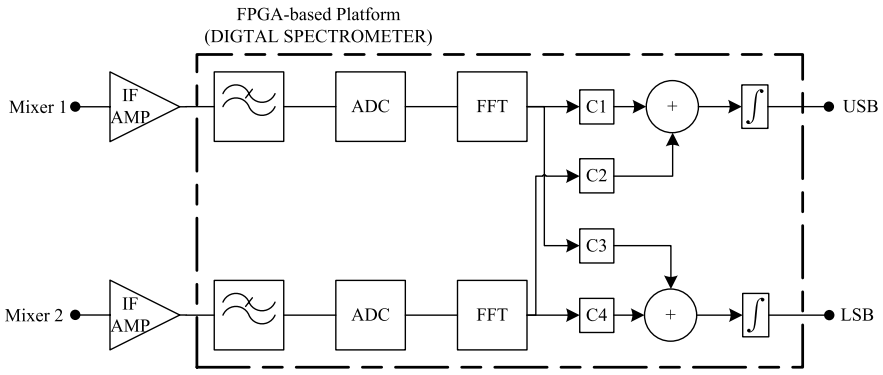

FIG. 2.—Configuration programmed inside the digital board. After the mixers and an amplification stage, the signals coming from the mixers are filtered by a low-pass filter and digitalized. Then, using the FPGA, the fast Fourier transform is calculated. Constants C1–C4 and the complex adders represent the digital IF hybrid which compensates the amplitude and phase imbalance in the system. These constants are determined by sweeping a tone through the whole RF band, and measuring the amplitude and phase imbalances of the analog part. The result is integrated and the USB and LSB spectra are obtained (3).

The new configuration presented here replaces the IF hybrid by a digital platform. This system is based on a Reconfigurable Open Architecture Computing Hardware (ROACH)[3] board (4) which includes two analog-to-digital converters ($3\ \mathrm{Gs\,s^{-1}}$), an Field Programming Gate Array (FPGA) for data processing, and a Performance Optimization With Enhanced RISC – Performance Computing (Power PC) to control data flow and interfaces with computing systems through Ethernet. At the input of the digital system, two IF amplifiers and low-pass antialiasing filters were added to reach the required signal levels and to clearly define the operation band. The system not only mimics the IF hybrid, but also serves as a spectrometer. Therefore, the output corresponds to the final integrated spectra of both sidebands. Its internal configuration is presented in Figure 2.

3. EXPERIMENT

Figure 3 presents a block diagram and a photograph of the setup used for measuring the sideband ratio. For comparison purposes, the sideband rejection ratio was first measured in the receiver using the analog IF hybrid and then using the digital version. To determine the sideband rejection ratio with the analog system, we used a spectrum analyzer. An RF signal was swept from $f_{LO} - IF_{\max}$ to $f_{LO} + IF_{\max}$, where $IF_{\max}$ is the bandwidth (3 GHz and 500 MHz in the analog and digital systems, respectively), and fed directly into the receiver, while the signal at one of the IF ports was measured with the spectrum analyzer. Then, the same sweep was repeated while measuring the spectrum at the second IF port. The ratio of the two spectra gives, then, the sideband rejection as defined in equation (1).

The measurement of the sideband rejection ratio when the receiver uses the digital IF spectrometer is similar. In this case, the spectrum analyzer is not needed as the outputs of the IF amplifiers are connected directly to the Analog-to-Digital Converter (ADCs) of the ROACH board. However, before measuring the sideband rejection, it is necessary to calibrate the spectrometer by obtaining the phase and amplitude imbalance between the amplified IF outputs of the mixers. In this way, the constants C1 to C4 (see Fig. 2) are obtained. This calibration must be performed every time the LO frequency or power are changed. It is important to notice that in the present paper we have defined the sideband rejection as the ratio between the tone in the desired sideband output to the largest tone in the other output (Finger et al. 2013). In the extreme case, the largest tone in the incorrect band can be a spurious tone. Therefore, this is a worst-case limit for the sideband rejection.

In order to test the calibration of the ROACH board, another measurement was performed with the board replaced by a Vector Network Analyzer (VNA). The difference of phase and amplitude between the IF ports of the mixers, namely IF1 and IF2, were measured using two different methods. The first was to measure the ports IF1 and IF2 by different channels without any attempt at performing a synchronized reading. The second was to measure simultaneously the two channels and, therefore, the complex ratio IF1/IF2 directly. Both were performed using internal functions of the VNA.

To measure the image rejection ratio, equation (2), one can either apply the procedure described in (Kerr et al. 2001) or introduce two signals at different RF sidebands producing the same IF frequency. The former requires only one RF input signal and measuring a wideband RF source at two different temperatures. The later requires a knowledge of the relative powers of the input signals. We have followed the second method. To determine the relative powers of two RF inputs at different frequencies, we have measured the RF power across the whole band as seen at the input of the RF hybrid. To achieve this, the RF coupling was maintained identical to the original experiment while the receiver was replaced by an Agilent N9030A spectrum analyzer.

[3] See https://casper.berkeley.edu/wiki/ROACH.

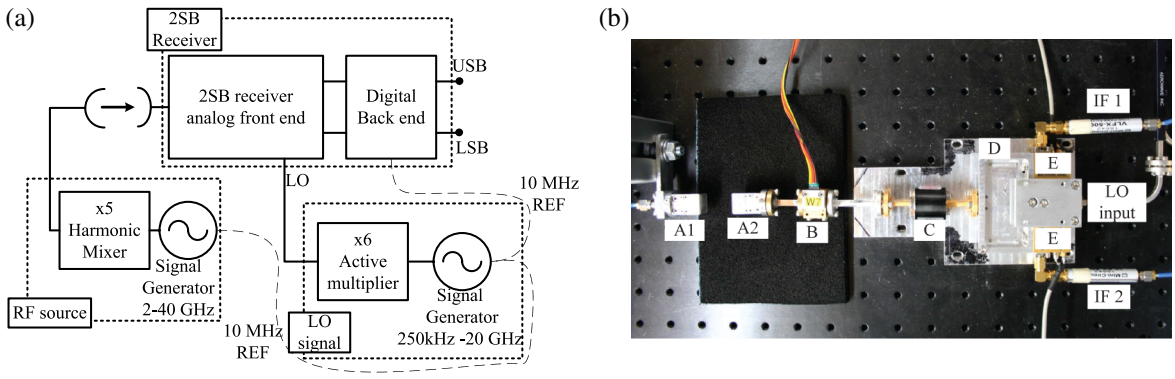

FIG. 3.—(*a*) Block diagram of the experimental setup. It includes the use of two signal generators with frequency multiplication in order to obtain frequencies around 100 GHz. The 10 MHz reference to the RF source is only used for calibration purposes. In the analog setup, a spectrum analyzer is used to measure the spectrum at one port (USB or LSB) at a time. When using the digital setup, the IF hybrid and the spectrometer are implemented in the ROACH-board. (*b*) Picture of the experimental setup showing the analog RF components: (*A*1) harmonic mixer and feed horn as RF source, (*A*2) horn, (*B*) LNA amplifier, (*C*) isolator, (*D*) RF hybrid, and (*E*) mixers. The LO input and IF outputs are also shown. See the online edition of the *PASP* for a color version of this figure.

All the measurements described in this section were performed with the receiver at room temperature (20° C). Therefore, the noise of the receiver is not optimal and it is only used to demonstrate the capabilities of the digital back end.

4. RESULTS AND DISCUSSION

Figure 4 presents the sideband rejection of the receiver with the analog IF hybrid. The sideband rejection is greater than 7 dB in the band of 84–100 GHz, in which the analog system can be measured. Notice that at different LO frequencies covering the same RF range the sideband rejection ratios are different. This is caused by mixers having different performance at different LO frequencies. No attempt was made to modify the bias of the mixers in order to improve the sideband rejection.

Figure 5*a* shows an example of the amplitude and phase imbalances measured with the digital spectrometer. From these values, the calibration constants are calculated. The measured values are rather noisy but a clear trend is visible which is drawn in solid lines. We attribute the origin of this noise to the fact that in the implementation of the digital spectrometer there is no timing control in the data acquisition from the ROACH board to the computer. This noise appears in the presence of large phase noise in the LO and test RF signals that propagates into the IF signal. In our case, in order to generate frequencies around 100 GHz, it was necessary to use multipliers for both the LO and RF signals, which increases the phase noise. Therefore, the phase of the signal at the two output ports could be completely unrelated since they could correspond to measurements made at different times. This is, evidently, increased with a higher phase noise. Indeed, such noise was not visible in our previous work (3).

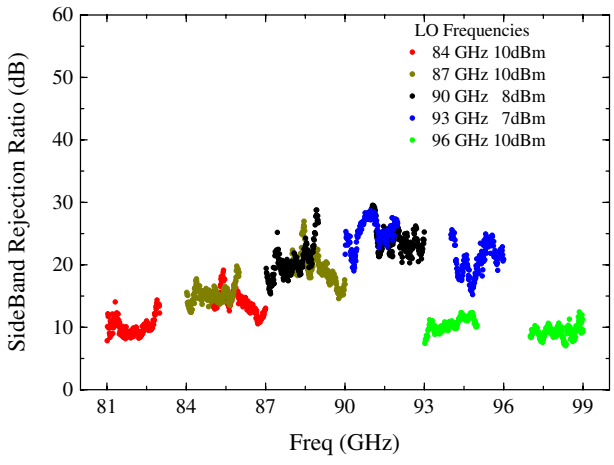

FIG. 4.—Sideband rejection ratio using an analog IF hybrid for different LO frequencies. The LO power was optimized for best mixer performance. See the online edition of the *PASP* for a color version of this figure.

In order to verify this hypothesis, the same measurement was repeated using a VNA, as explained in § 3. An example of such measurements is shown in Figure 5*b*. When the measurements are done without any synchronization between ports IF1 and IF2 (*gray dots*), noise appears in the phase and amplitude imbalances. This noise is very similar to the one appearing in the measurements performed with the ROACH-based spectrometer. On the other hand, when the measurements are synchronized (*black dots*), i.e. obtained at the same time, the noise disappears altogether. Having thus confirmed our hypothesis, a synchronization block was programmed inside the digital spectrometer. This block prevents the incoming stream of data from entering to the memories while the data are being read by the computer. The calibration data with this improvement is presented in Figure 5*c*. The new calibration data are identical to the trend lines presented in Figure 5*a*, but without any noise in the measurement.

In the next step we have measured the sideband rejection of the receiver using the digital spectrometer with the synchronization block. The results are presented in Figure 6*a*. Rejections

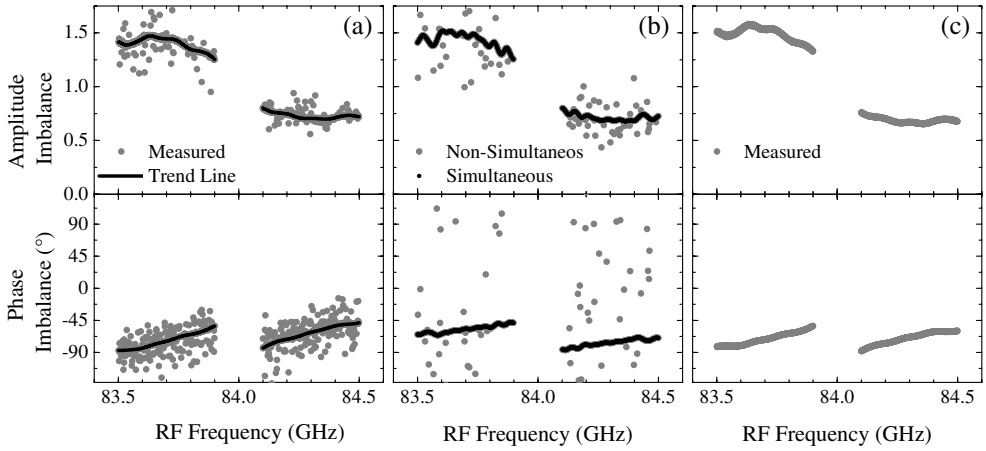

FIG. 5.—Amplitude and phase imbalances for a LO of 84 GHz. (*a*) Results of unsynchronized measurements with the digital spectrometer (*gray circles*) and their trend lines (*black lines*). (*b*) Results obtained with a VNA. The measurements were performed by reading simultaneously (*black lines*) and nonsimultaneously (*gray dots*) the two IF ports of the mixers. Notice that the measurements performed with our ROACH-based spectrometer and the VNA are not exactly the same. There is an additional path difference when using the latter, as an extra adapting cable had to be introduced in both paths. (*c*) Results of synchronized measurements with the digital spectrometer.

around 50 dB are obtained at the center of the band degrading to 35 dB at the edges. This degradation does not originate in the procedure presented here but in the degradation of the dynamic range of the setup due to a reduction in the conversion gain of the mixers. To illustrate this situation, in Figure 6*b* we present typical spectra obtained during the frequency sweep in the determination of the sideband rejection after calibration. As explained in § 3, we define the sideband ratio as the ratio between the tone in the correct sideband output (peak A) to either the tone in the incorrect output (peak B) or the highest spurious tone (peak C), whichever is larger. Evidently, the conversion gain of the mixers deteriorates at the band edges resulting in a lower peak A and, consequently, lower sideband ratio. The spurious tones are produced within the ADC chip and are the results of complex processes in the digital hardware. According to the datasheet, the ADC spurious tones of the chip used in these experiments (NI-ADC083000) are -50 dBc, for a full scaled (0 dBm) test tone. Therefore, 50 dB is the upper limit for signal rejection using this hardware.

Finally, we have also determined the image rejection ratio from the same set of data recorded when measuring the results presented in Figure 6*a*. Therefore, no extra calibration is required but a characterization of the RF input power is needed (Fig. 7*a*). The calculated image rejection ratios are presented in Figure 7*b*. They are also above 35 dB over the whole RF band of the receiver. At this point, it is necessary to remark that the calibration of the sideband separating receiver (i.e., determining the constants C1–C4) characterizes the receiver independently of whether R or r are measured or the method used to obtaining them.

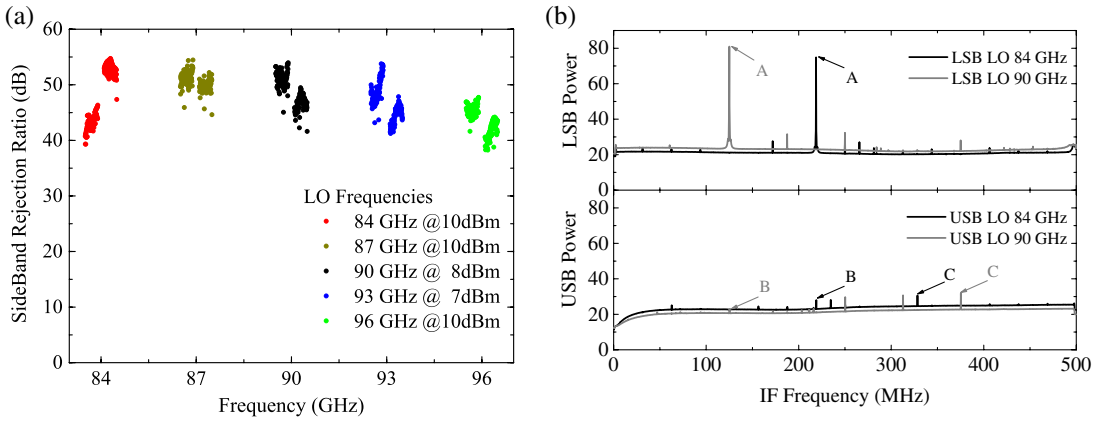

FIG. 6.—(*a*) Sideband rejection ratio for different LO frequencies using the digital spectrometer with synchronized data acquisition. (*b*) Typical spectra in the spectrometer while the sideband rejection is calculated. Peaks A, B, and C correspond to the tone in the correct sideband output, the tone in the incorrect output, and the highest spurious tone in the incorrect output, respectively. The sideband ratio is taken as the ratio between peak A and the highest between peaks B and C. The degradation in the sideband ratio is a consequence of the decrease in the amplitude of peak A. See the online edition of the *PASP* for a color version of this figure.

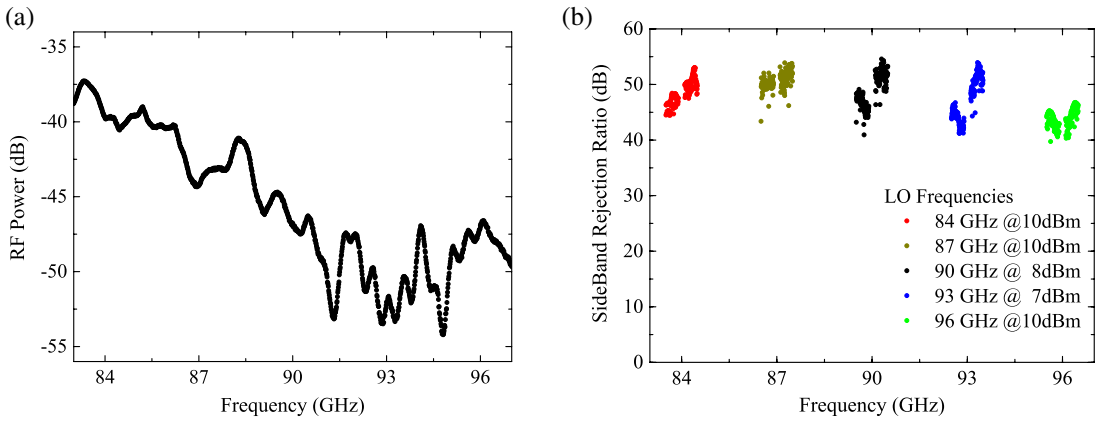

FIG. 7.—(*a*) Characterization of the RF power at the input port of the receiver using a an Agilent model N9030A spectrum analyzer. (*b*) Image rejection ratio for different LO frequencies with the corresponding LO power using the digital spectrometer with synchronized data acquisition. See the online edition of the *PASP* for a color version of this figure.

5. CONCLUSIONS

We have implemented a calibrated digital IF hybrid in a millimeter-wave receiver. In contrast with the values obtained when an analog IF hybrid is used, we have achieved image rejections of 50 dB at the center of the RF band with degradation at the band edges, but always above 35 dB. This degradation does not, however, originate in the digital hybrid but in the degradation of the dynamic range due to a reduction in the conversion gain of the mixers. It is important to note that we have used two commercial mixers whose conversion gains were not deliberately matched. We envision that using the technique presented here, matching the gain of mixers to be used as 2SB converters will not be needed. This demonstrates the enormous potential that digital platforms have for astronomical instrumentation. Finally, we have also demonstrated that it is important to have a properly synchronized acquisition of data in order to avoid that the phase noise present in the system affects the calibration of the receiver.

We would like to acknowledge the Center of Excellence in Astrophysics and Associated Technologies (CATA) PFB06, Gemini-CONICYT Fund 32120004, Fondecyt Project 1121051, and Programa de Formación de Capital Humano Avanzado of CONICYT for their financial support. We would also like to thank J. Pizarro for his help and advice in the construction of the mechanical parts.

REFERENCES

Claude, S. M. X., Cunningham, C. T., Kerr, A. R., & Pan, S.-K. 2000, ALMA Memo #316 (Charlottesville: National Radio Astronomy Observatory)

Dindo, P., Claude, S., Derdall, D., Henke, D., Erickson, D., Rodrigues, G., Lichtenberger, A., & Pan, S.-K. 2005, in Joint 30th Int. Conf. on Infrared and Millimeter Waves and 13th Int. Conf. on Terahertz Electronics, (IEEE)409–410

Finger, R., Mena, P., Reyes, N., Rodriguez, R., & Bronfman, L. 2013, PASP, 125(925) 263–269

Kerr, A. R., Pan, S.-K., & Effland, J. E. 2001, ALMA Memo #357 (Charlottesville: National Radio Astronomy Observatory)

Kooi, J. W. 2008, Ph. D. thesis, Univ. of Groningen

Mahieu, S., et al. 2012, IEEE Trans. Terahertz Sci. Technol., 2(1), 29–39

Maier, D., Reverdy, J., Billon-Pierron, D., & Barbier, A. 2012, IEEE Trans. Terahertz Sci. Technol., 2(2), 215–221

Mena, F. P., et al. 2011, IEEE Trans. Microwave Theory Tech., 59(1), 166–177

Morgan, M., & Fisher, J. R. 2010, PASP, 122(889), 326–335

Rodríguez, R., Finger, R., Vásquez, P., Bustos, R., Reyes, N., Zorzi, P., Bronfman, L., & Mena, F. P. 2012, Proc. SPIE, 8452, 845231–7

Sobis, P. J. 2011, IEEE Trans. Terahertz Sci. Technol., 1(2), 403–411

Vassilev, V., Belitsky, V., Risacher, C., Lapkin, I., Pavolotsky, A., & Sundin, E. 2004, IEEE Microwave Wireless Compon. Lett., 14(6), 256–258